Buletin Ilmiah Sarjana Teknik Elektro
Vol. 8, No. 4, August 2026, pp. 1236-1258
ISSN: 2685-9572, DOI: 10.12928/biste.v8i4.16847

Active Disturbance Rejection and Model Predictive Control for Mitigating Non-Torque-Producing Currents and Harmonic Distortion in Six-Phase Permanent Magnet Synchronous Motor

Rjwan Ahmed Al-Hamdany [1], Jameel Kadhim Abed [2], Mustafa Naozad Taifor [3], Sarah A. Mohammed [4], Ali Falih Challoob [5], Naseer T. Alwan [6,7], Salam J. Yaqoob [8]
[1] Northern Technical University, Iraq/ Technical Engineering College – Kirkuk, Kirkuk 36001, Iraq
[2] Department of Power Engineering, AL-Hikma University College, Baghdad 10001, Iraq
[3] Renewable Energy Research Center- Kirkuk, Northern Technical University, Kirkuk 36001, Iraq
[4] Electrical Engineering Technologies, Al-Furat Al-Awsat Technical University, Babil 51006, Iraq
[5] Institute of Power Engineering, Universiti Tenaga Nasional (UNITEN), Malaysia
[6] Renewable Energy Research Center - Kirkuk, Northern Technical University, Kirkuk, 36001, Iraq
[7] Ural Federal University named after the first President of Russia B. N. Yeltsin, 19 Mira St., Yekaterinburg, Russia
[8] Training and Energy Research Office, Ministry of Electricity, Baghdad 10001, Iraq

ARTICLE INFORMATION

Article History:

Received 22 May 2026
Revised 04 August 2026
Accepted 05 September 2026

Keywords:

PMSM;
Model Predictive Control;
Total Harmonic Distortion;
MATLAB/Simulink;
Vector Space Decomposition

Corresponding Author:

Salam J. Yaqoob,
Training and Energy Research Office, Ministry of Electricity,
Baghdad 10001, Iraq.
Email: engsalamjabr@gmail.com

ABSTRACT

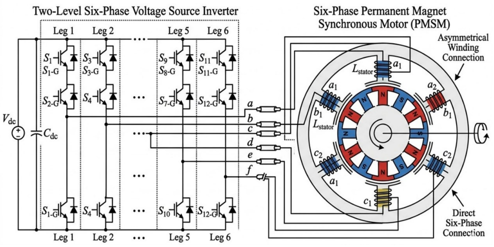

The six-phase permanent magnet synchronous motor drives have high power density, fault tolerance, and reliability; however, conventional model predictive control is sensitive to load disturbances, unmodeled dynamics, and parameter uncertainties, which can lead to high non-torque-producing currents and harmonic distortion. To overcome these drawbacks, this work introduces an active disturbance rejection control approach with model predictive control (MPC). The research contribution is the combination of active disturbance estimation and compensation in the outer speed loop with the predictive current regulation in the inner current loop to improve disturbance rejection, reduce non-torque-producing currents, and improve the dynamic performance of the six-phase motor drives. The proposed scheme is modeled and validated through the MATLAB/Simulink simulation and compared to the standard MPC at the speed reference of 1000 rpm, load-torque steps of 10N·m applied in 0.05 s and 15N·m applied in 0.1 s, and motor inertia of 0.0048 kg·m². The simulation results show the current THD is reduced to 2.3% with the proposed strategy, and the average switching frequency is diminished to 10.8 kHz. The peak transient torque error is reduced from 0.65 N · m to 0.10 N · m, and steady-state torque ripple is lessened from 0.15 N·m to 0.02 N·m. Furthermore, the maximum speed deviation is lowered from about 150 rpm to 35 rpm, and the recovery time after a load disturbance is lowered from 40ms to 10ms. The obtained outcomes demonstrate the dominance of harmonic suppression, disturbance rejection, and dynamic efficacy of the proposed approach, indicating its prospective use in high-performance multiphase electric-drive systems.

Document Citation:

R. A. Al-Hamdany, J. K. Abed, M. N. Taifor, S. A. Mohammed, A. F. Challoob, N. T. Alwan, and S. J. Yaqoob, "Active Disturbance Rejection and Model Predictive Control for Mitigating Non-Torque-Producing Currents and Harmonic Distortion in Six-Phase Permanent Magnet Synchronous Motor," *Buletin Ilmiah Sarjana Teknik Elektro*, vol. 8, no. 1, pp. 1236-1258, 2026, DOI: 10.12928/biste.v8i4.16847.

1. INTRODUCTION

The extreme efficiency, extreme capacity density, fast active response, and wonderful torque characteristics of the (PMSM) drives have made them as one of the most common engine technologies in today's technical and transportation worlds. The above benefits render PMSM drives especially appealing in electric vehicles, aerospace propulsion, ship propulsion, robotics, and renewable energy conversion systems. Most PMSM drive systems are historically three-phase, although in recent years, multiphase machine drives have been receiving growing interest because of their superior reliability, increased fault tolerance, smaller torque ripple, and increased power density [1]. These multiphase topologies, six-phase PMSMs, have become a possible solution in high-performance and safety-critical uses. The 6-phase PMSM drive system has a number of benefits over the traditional three-phase drives. Using more stator phases, the system is able to spread the power more efficiently and lessen the current stress on each stator phase. Also, multiphase systems are naturally redundant, providing the capability to still operate even when there is a fault on one or more phases. It is especially significant in mission-critical applications, like electric aircraft propulsion, ship propulsion, and electric vehicle traction systems, where system reliability is paramount. Moreover, multiphase machines have the capacity to significantly lower the torque pulsations and enhance electromagnetic operation because of the added degrees of freedom of control of current [2][3].

Although specific benefits are savored, skilled challenges are any of the challenges in the control of a six-time PMSM. Phases increase the range of bureaucracy and the complexity of the vital presence of bureaucracy, as distinguished from three-point arrangements. Besides, multiphase machines may bring more subspaces to the framework of the vector space decomposition (VSD), and they need to be properly regulated to avoid undesired harmonic currents and performance losses. Consequently, sophisticated control measures are needed to utilize the advantage of 6-phase PMSM drives to the maximum and provide stable and high-performance operation.

The most commonly used control PMSMs are consistently field-oriented control (FOC) and direct torque control (DTC). However, FOC is sensitive to machine parameter accuracy and needs several cascaded control loops, demanding more complex systems and reducing dynamic response. In addition, the changes in limits, exogenic shocks, and forming errors can have a harsh decaying effect on the conduct of FOC-located systems [4]. DTC suggests a less complex building of control and a smaller collar reaction than FOC. However, DTC has several restraints, including the changing exchange frequency, extreme collar ripple, and exaggerated current deformity. These problems are even more magnified in multiphase PMSM systems since they have even more dimensions of control. As a result, a greater number of sophisticated control approaches have been investigated to overcome these shortcomings and enhance the overall functionality of PMSM drives [5]. The MPC is a recently used advanced control program to power electronic converters and electric drives. Among other benefits, MPC has fast dynamic reaction, multivariable systems, and the object of system constraints can be directly included in the control algorithm. Compared to conventional methods of control based on cascade control loops and pulse-width modulation (PWM), MPC anticipates directly the future system behavior created on a mathematical model and optimizes the control action by decreasing an established objective function [6]

However, FCS-MPC is capable of managing a variation of variables at the same time, containing torque, flux, and current elements, and it is especially applicable in multiphase PMSM systems [7]. Nonetheless, model predictive control has several challenges in spite of its benefits. The high demand for the accuracy of the system model is one of the most vital ones. PMSM drive systems are vulnerable to several uncertainties in practice, including inaccurate parameters, disruptions in loads, nonlinearities of inverters, and unmodeled dynamics. Such ambiguities are causing errors in the prediction and control performance of MPC-based systems [8]. Thus, it has turned out to be a significant research direction to enhance the resilience of MPC to disturbances and model mismatch. DOB methods have been extensively applied in control systems to assess and counterbalance the unknown disturbances and model uncertainty. A disturbance observer operates by measuring the overall disturbance on the system in terms of the difference between the measured output and the nominal model-predicted output. The disturbance is assessed and used to offset the control input, hence enhancing system robustness and disturbance rejection authority [9]. Recently, commotion spectator integration accompanying MPC has resulted in an efficient system to correct the robustness of MPC-located plans. The introduction of commotion guess into the predictive model will allow the boss to counter external disturbances in addition to shaping errors in real-time for action or event. The mixture solution is an association of extreme dynamic response and restraint management conduct of MPC and good commotion rejection performance of upset spectators. The use of disturbance-observer-based MPC has the potential to be of great benefit in the context of 6-phase PMSM drives [10]. Therefore, the disturbance observer is capable of estimating some unknown disturbances, including load torque variations, mismatch of parameters, and nonlinearities in inverters. Second, the predicting model may be reinforced by judging the disturbances and including bureaucracy in the predicting model to form the indicators more accurately and to enhance the effectiveness of the control. Third, the suggested approach can be used to adequately suppress undesirable harmonic currents in the extra subspaces of the six-phase system and, consequently, enhance the overall drive efficiency and torque quality.

The other major point of multiphase PMSM control is the VSD scheme. VSD is typically applied to derive the stator variables of 6 phases into a series of orthogonal subspaces, typically the fundamental α subspace, the secondary harmonic subspace, and the zero-sequence subspace. The $\alpha - B$ subspace is the one that constructs torque with all the other subspaces, chiefly carrying harmonic components that do not contribute to the torque production. There should then be effective control mechanisms that control the currents in these subspaces to ensure that harmonic losses are kept to a minimum to enhance efficiency in these systems [11]. MPC offers a convenient model to control several subspaces at a time. MPC can also achieve the best current tracking and harmonic suppression by incorporating the existing elements of various subspaces into the cost function. Nevertheless, even in the situation when the disturbances and parameter uncertainties do not have a major influence on the predictive accuracy, the control performance will still be hurt. Consequently, a disturbance observer must be incorporated into the MPC model to enhance the resilience and dependability of the control approach. In recent studies, numerous MPC-based controls of multiphase PMSM drives have been studied [12]. To illustrate, predictive current control systems have been suggested to directly control the stator currents, and predictive torque control systems to obtain rapid torque reaction and reduced torque ripple. Also, some studies have been done on multiple-objective cost functions to achieve the maximum control of torque performance, switching frequency, and harmonic suppression at the same time. However, most of these methods are yet again based on precise machine models and can be affected by the presence of disturbances or variations of parameters [13][14]. To overcome these issues, MPC strategies that utilize disturbance observers have been proposed in several applications in motor drives. These methods generally use a prolonged state viewer or a sliding mode disturbance viewer to approximate the lumped disturbances in the system. The presentation of the estimated disturbances is then added to the predictive model to improve the robustness of the predictive model to be robust and reject disturbances. Nevertheless, the majority of the available literature is concentrated on three-phase motor drives, and comparatively few papers have examined disturbance-observer-based MPC on six-phase PMSM systems. With the growing need for high-reliability and high-performance electric drive systems, the design of robust control techniques for multiphase PMSM drives is a significant research topic. Specifically, postponement observer procedures and model anticipatory regulation are a plausible solution to enhancing the robustness, dynamic execution, and disturbance rejection capacity of 6-phase PMSM drive systems [15]. To enhance the robustness and harmonic rejection of predictive control strategies for PMSM and multiphase drives, recent studies have been directed towards improving the computational ability. To overcome the sensitivity of traditional predictive controllers due to the mismatch of model parameters and unmodeled disturbances, recent model-free predictive current control methods have been developed using a sliding-mode disturbance observer [16]. In the same way, the lumped disturbance compensation of model predictive current control with a sliding mode disturbance observer has been analyzed to improve the current prediction accuracy [17]. For six-phase PMSM drives, recent predictive current control algorithms have been designed for the steady-state performance as well as the control of extra current subspaces of the multiphase machine [18]. For a dual 3-phase PMSM, prediction-based current control of models without a model analysis is developed to mitigate the influence of the model on the performance of the drive and improve the performance of current control [19]. Other recent advancements have led to the incorporation of extended-state-observer-assisted and weightless predictive control structures, which decrease the sensitivity of the controller to parameter perturbations and make it easier to select the weighting factors [20]. More recently, predictive current control with explicit harmonic suppression has been proposed for explicit harmonic suppression and to target specific current harmonics, thereby lowering total harmonic distortion [21]. However, simultaneous disturbance rejection, accurate regulation of the torque-producing currents, suppression of the non-torque-producing subspace currents, and controlled switching activity are still difficult tasks, especially for a 6-phase PMSM. This restriction is a motivation for the research on integrating active disturbance estimation and predictive current control discussed in the present work.

1.1. Research Gap

Although the PMSM drives have overcome many challenges in predictive control and disturbance-rejection control, there are still some difficulties that need to be solved in the 6-phase drive. However, conventional MPC is based on machine models that must be accurate and may suffer in terms of current and speed regulation if there are parameter changes, unmodeled dynamics, or sudden load changes. Furthermore, the extra degrees of freedom provided by the 6-phase topologies result in no torque-producing x−y current components, which must be explicitly controlled in the predictive control objective. Current approaches based on ADRC have been utilized to accurately evaluate the disturbance and compensate for it, but have not been developed to solve the problem of discrete voltage-vector selection and the control of harmonic currents in multiphase subspaces. On the other hand, conventional MPC can directly control a number of current components, but the disturbance-rejection capability relies on the accuracy of the prediction model. Hence, a control scheme that integrates active disturbance estimation and predictive regulation of torque-creating and non-torque-creating current components is needed. To fill this gap, the proposed six-phase PMCS strategy for PMCS drives has been developed.

1.2. Research Contribution

The research contribution is a novel active disturbance estimation-based outer speed-control loop along with the finite-control-set predictive current regulation-based inner control loop, forming an integrated ADRC-MPC control framework for six-phase PMSM drives. The proposed architecture differs from the conventional MPC in that the lumped disturbances to the speed regulation are estimated and compensated, and the predicted values of the current components that can be generated to produce torque are explicitly controlled, whilst the non-torque-producing components of the x−y current are explicitly rejected by the control objective. Robustness against external disturbances and model uncertainties, and harmonic current regulation in the additional subspaces of six-phase machines, are thus two complementary problems considered here. The contribution is compared with conventional MPC under a set of similar simulated operating conditions in terms of speed response, torque tracking, current harmonic distortion, current decoupling, and switching activity.

1.3. Paper Organization

The rest of this article is arranged as shadows. In Partition 2, the mathematical modeling of the six-phase PMSM is introduced, which involves vector space decomposition and the representation of the subspaces of the torque-producing and non-torque-producing currents. In Section 3, the conventional model predictive control strategy is presented, and the predictive current-control formulation is described. The proposed ADRC-MPC framework is introduced in Section 4, which consists of a disturbance estimation mechanism, speed-loop control, and a predictive cost-function formulation. Results of MATLAB/Simulink simulation and discussion of the results appear and are discussed in Partition 5, and comparative performance evaluation of conventional MPC and proposed ADRC-MPC strategy is demonstrated in Partition 5. Lastly, Partition 6 presents the key results of the current study, identifies its limitations, and proposes ideas for further research.

2. MATHEMATICAL MODELING OF 6-PHASE PMSM

2.1. Modeling of 6-Phase PMSM

A 6-phase PMSM is often constructed from two groups of 3-phase stator windings, spatially displaced by 30 electrical degrees. These windings are either linked to a dual three-phase inverter or a six-leg voltage source inverter. The benefits of the multiphase makeup include higher dependability, lower armband ripple, and error resistance [22][23]. To examine and manage the six-phase PMSM, the stator variables are typically converted into orthogonal subspaces relative to the six-phase fixed frame by VSD. This approach separates the torque-producing components from the harmonic components [24]. The stator voltage equations of the six-phase PMSM in the phase-organized system can be expressed as

$$v_s = R_s i_s + \frac{d\psi_s}{dt} \tag{1}$$

where $v_s = [v_{a1}, v_{b1}, v_{c1}, v_{a2}, v_{b2}, v_{c2}]^T$ is the stator voltage vector, $i_s = [i_{a1}, i_{b1}, i_{c1}, i_{a2}, i_{b2}, i_{c2}]^T$ is the stator current vector, $R_s$is the stator phase resistance, ψ_s Is the stator flux linkage vector.

The stator flux linkage can be written as

$$\phi_s = L_s i_s + \phi_m \tag{2}$$

where $L_s$is the stator inductance matrix, ϕ_m represents the flux linkage.

Because of the complexity of the six-phase system, direct analysis in the phase domain is difficult. Therefore, coordinate transformations are applied [25][26]. The 6-phase system can be transformed into 3 orthogonal subspaces: $\alpha - \beta$ subspace (torque producing), $x - y$ subspace (harmonic subspace) and zero-sequence subspace.

The transformation from six-phase variables to orthogonal subspaces can be written as

$$i_{vsd} = T_6 i_s \tag{3}$$

where T_6Is the transformation matrix. The resulting current vector becomes:

$$i_{vsd} = [i_\alpha, i_\beta, i_x, i_y, i_{z1}, i_{z2}]^T \tag{4}$$

The $\alpha - \beta$ components correspond to the fundamental torque-producing components, while the $x - y$ components represent harmonic currents that do not contribute to torque [27]. To simplify the mechanism, the $\alpha - \beta$ components are further changed into the synchronous rotating d-q orientation frame utilizing the Park conversion:

$$\begin{bmatrix} i_d \\ i_q \end{bmatrix} = \begin{bmatrix} cos\,\theta_e & sin\,\theta_e \\ -sin\;\theta_e & cos\,\theta_e \end{bmatrix} \begin{bmatrix} i_\alpha \\ i_\beta \end{bmatrix} \tag{5}$$

where θ_eIs the electrical rotor position, in the same way, voltages are transformed as:

$$\begin{bmatrix} v_d \\ v_q \end{bmatrix} = \begin{bmatrix} cos\,\theta_e & sin\,\theta_e \\ -sin\;\theta_e & cos\,\theta_e \end{bmatrix} \begin{bmatrix} v_\alpha \\ v_\beta \end{bmatrix} \tag{6}$$

The voltage equations of the 6-phase PMSM in the synchronous d-q frame are articulated as:

$$v_d = R_s i_d + \frac{d\psi_d}{dt} - \omega_e \psi_q \tag{7}$$

$$v_q = R_s i_q + \frac{d\psi_q}{dt} + \omega_e \psi_d \tag{8}$$

where v_d, v_q are the stator voltages in the d-q frame? i_d, i_q are the stator currents, ω_e is the electrical angular speed.

The flux linkages are:

$$\psi_d = L_d i_d + \psi_f \tag{9}$$

$$\psi_q = L_q i_q \tag{10}$$

where L_d, $L_q$are the d- and q-axis inductances, ψ_f The flux linkage in the $x - y$ subspace represents harmonic components that do not contribute to torque creation but may cause additional losses.

The voltage equation as follows:

$$v_x = R_s i_x + L_{xy} \frac{di_x}{dt} \tag{11}$$

$$v_y = R_s i_y + L_{xy} \frac{di_y}{dt} \tag{12}$$

where i_x and , $i_y$are harmonic currents; L_{xy} Is the harmonic subspace inductance.

Moreover, proper control strategies aim to keep these currents close to zero to reduce harmonic losses [28]. The torque of the six-phase PMSM is consequent from the interaction between the stator currents and rotor flux.

$$T_e = \frac{3}{2} p[\psi_f i_q + (L_d - L_q) i_d i_q] \tag{13}$$

where T_e is the torque, p is the number of pole pairs. For a surface-mounted PMSM, where $L_d = L_q$, the torque simplifies to

$$T_e = \frac{3}{2} p \psi_f i_q \tag{14}$$

Thus, torque can be controlled directly by regulating the q-axis current. The mechanical dynamics of the motor are described by

$$J\frac{d\omega_m}{dt} = T_e - T_L - B\omega_m \tag{15}$$

Where J is the rotor inertia, $\omega_m$is the mechanical speed, T_L is the load torque, B is the viscous friction coefficient.

The relationship between electrical and mechanical speed is:

$$\omega_e = p\omega_m \tag{16}$$

2.2. Structure of 6-Phase PMSM

Figure 1 shows that a 2-level 6-phase Voltage Source Inverter (VSI) is a key component in six-phase PMSM drive systems. It converts a DC input voltage into a controlled six-phase AC output, which supplies the stator windings of the motor. In MPC-based drives, the inverter plays a critical role because its discrete switching states are directly used in the control algorithm [29][30]. For a six-phase inverter, the switching vector is:

$$S = [S_{a1}, S_{b1}, S_{c1}, S_{a2}, S_{b2}, S_{c2}] \tag{17}$$

where each $S_i \in \{0,1\}$. $2^6 = 64$ switching states. The general voltage vector:

$$S\vec{v} = v_\alpha + jv_\beta \tag{18}$$

where: $v_\alpha = \frac{2}{6}V_{dc}\sum_{k=1}^{6} S_k \cos\ \theta_k$, $v_\beta = \frac{2}{6}V_{dc}\sum_{k=1}^{6} S_k \sin\ \theta_k$

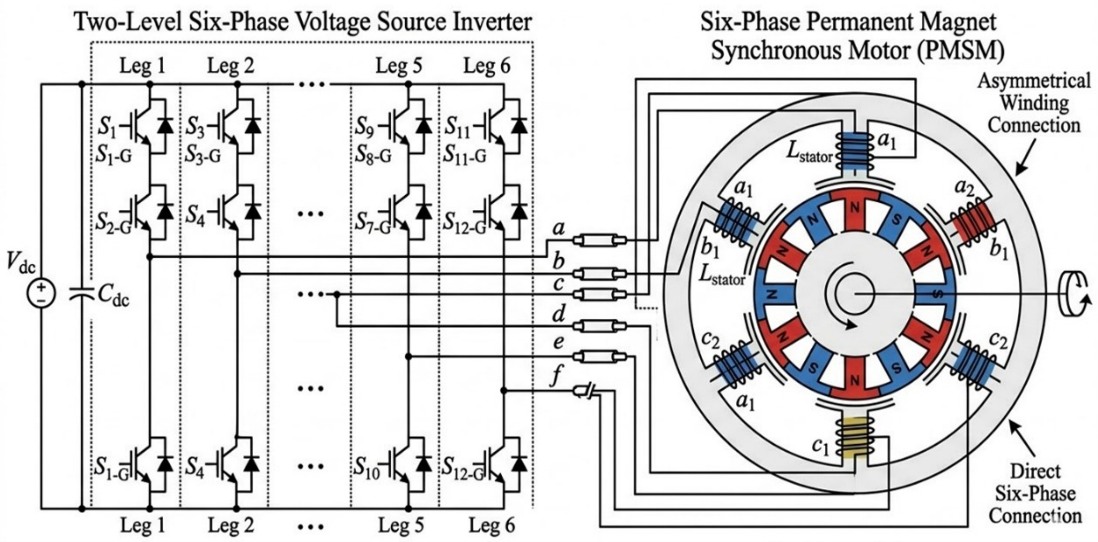

Figure 1. Structure of the Six-Phase PMSM

2.3. Model Predictive Control of PMSM

MPC is a modern mechanism that has enjoyed considerable popularity in electric drive systems since it possesses rapid dynamic response, easy architecture, and multivariate systems and constraints [31][32]. In PMSM drives, the Model Predictive Control (MPC) uses the numerical model of the motor to predict the future behavior of the scheme and to choose the optimal voltage vector by minimizing a specific cost function. The control structure is simpler than in FOC, since the MPC does not need cascaded current controllers and PWM modulation, and it improves the control dynamics [33].

2.4. Principle of MPC

The essential impression of MPC is to predict the future states of the system for all conceivable switching states of the inverter and then choose the switching state that lessens an objective function [34][35]. The objective function represents the control objectives, such as minimizing current tracking error, torque ripple, or switching frequency. The MPC control process typically consists of the following steps:

1. Measure stator currents and rotor position.
2. Use the motor model to predict future currents for each inverter switching state.
3. Estimate the objective function for each predicted state.
4. Choose the switching state with the minimum cost.
5. Utilize the corresponding voltage vector of the inverter.

This procedure is recurrent at every sampling period.

2.5. Mathematical Model of PMSM Under MPC

In predictive control, the PMSM model is typically expressed in a synchronous $d - q$ orientation frame [36]. The stator voltage equations are defined as follows:

$$v_d = R_s i_d + L_d \frac{di_d}{dt} - \omega_e L_q i_q \tag{19}$$

$$v_q = R_s i_q + L_q \frac{di_q}{dt} + \omega_e \left(L_d i_d + \psi_f\right) \tag{20}$$

In MPC, the objective function plays a central role in deciding the optimal switching state of the inverter. The cost function evaluates the predicted behavior of the motor for each candidate voltage vector and selects the control action that minimizes the control error according to predefined objectives [37]. In 6-phase PMSM drives, the objective function design is more complicated than in 3-phase systems because several current subspaces have to be operated at once. Using VSD, a six-phase PMSM system can be broken down into a set of orthogonal subspaces: there is the VSD -b subspace, which generates electromagnetic torque, the VSD x-y harmonic subspace, which contains non-torque-generating harmonic components, and the zero-sequence subspace [38]. Effective cost function design must ensure accurate current tracking in the torque-producing subspace while suppressing harmonic currents in the other subspaces [39]. The cost function of the predictive controller is designed to satisfy several control objectives simultaneously:

1. Correct tracking of the orientation currents in the torque-producing subspace.
2. Suppression of harmonic currents in the secondary subspaces.
3. Reduction of switching frequency to improve efficiency.
4. Minimization of torque ripple and current distortion.

These objectives are incorporated into the objective function through weighted error terms. Before evaluating the objective function, the controller predicts the stator currents at the next sampling instant using the discrete model of the 6-phase PMSM [40][41]. The motor equations are then discretized using the forward Euler approximation for a sampling period Ts to implement the continuous-time model of the six-phase PMSM in the finite-control-set MPC framework. The dynamics of the $d - q$ currents obtained from Eq. (19) and Eq. (20) can be articulated as follows:

$$\frac{di_d}{dt} = \frac{1}{L_d}\left(v_d - R_s i_d + \omega_e L_q i_q\right) \tag{21}$$

$$\frac{di_q}{dt} = \frac{1}{L_q}\left[v_q - R_s i_q - \omega_e (L_d i_d + \psi_f)\right] \tag{22}$$

The predicted currents in the synchronous d-q frame are

$$i_d(k+1) = i_d(k) + \frac{T_s}{L_d}(v_d - R_s i_d + \omega_e L_q i_q) \tag{23}$$

$$i_q(k+1) = i_q(k) + \frac{T_s}{L_q}(v_q - R_s i_q - \omega_e (L_d i_d + \psi_f)) \tag{24}$$

Similarly, the predicted currents in the harmonic subspace are:

$$i_x(k+1) = i_x(k) + \frac{T_s}{L_{xy}}(v_x - R_s i_x \quad (25)$$

$$i_y(k+1) = i_y(k) + \frac{T_s}{L_{xy}}(v_y - R_s i_y) \quad (26)$$

where T_s is the sampling period, R_s is the stator resistance, $L_d, and\ L_q$ are dq inductances, L_{xy} Is the harmonic inductance.

The FCS-MPC algorithm computes the candidate voltage vectors of the six-phase inverter for each sampling time k. The above set of discrete-time equations is used to predict the corresponding d−q and x−y currents at k+1 for each candidate vector.

The predicted currents are then used to substitute for the objective function, and the switching state that lessens the cost is selected and utilized at the next sampling time [42]. These predicted currents are then used in the objective function. The simplest objective function focuses on lessening the error between the orientation and predicted currents in the torque-producing subspace.

$$= (i_d^* - i_d(k+1))^2 + (i_q^* - i_q(k+1))^2 \quad (27)$$

where $i_d^*, and\ i_q^*$ are the reference currents. In surface-mounted PMSM drives, the reference current is usually. $i_d^* = 0$ used because torque is mainly controlled through the q-axis current.

In six-phase PMSMs, the $x - y$ subspace currents do not contribute to torque but may generate additional copper losses and harmonic distortion. Therefore, these currents should ideally be maintained close to zero. The weighting factor λxy sets the relative priority of suppressing the non-torque-producing $x - y$ currents with respect to d−q current tracking [43][44]. The higher λxy is, the higher the harmonic-current suppression level, but the worse the dynamic tracking of the torque-generating current components will be. Hence, λxy is chosen to achieve a compromise between minimizing the error in tracking the d current and the x and y currents. It is important to note that ADRC does not directly and perfectly decouple the $x - y$ subspace; ADRC improves the disturbance rejection performance in the speed-control loop, and the MPC cost function explicitly controls the non-torque-producing current components. To achieve this objective, additional terms are added to the cost function:

$$g = (i_d^* - i_d)^2 + (i_q^* - i_q)^2 + \lambda_{xy}(i_x^2 + i_y^2) \quad (28)$$

where $\lambda_{xy}$is a weighting factor that controls the importance of harmonic suppression. A larger value of λ_{xy} Results in stronger suppression of harmonic currents. Figure 2 shows how the controller predicts the motor behavior and selects the best switching indications for the inverter in real time.

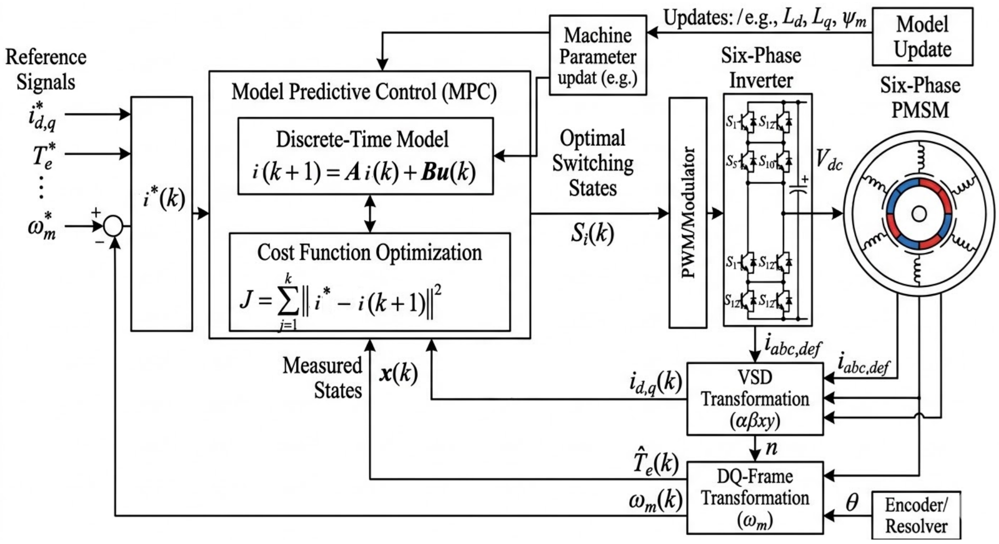

Figure 2. Block diagram of the MPC of a 6-phase PMSM

2.6. Active Disturbance Rejection Control of PMSM

2.6.1. Design of ADRC strategy

In comparison to simple PI control, ADRC demands presenting certain regulated news during the mechanism process, that is, the order of the regulated aim, the moment of truth scale, that is, the speed of change, etc. Concurrently, it has the merits of being smooth to rule, behaving fast, and bearing good anti-upset properties [45]. When a state spectator is operating, the first news expected to be noticed by the state spectator is the state facts of each response quantity and the upset mistake facts, along with the control of the regulated object. It, in proper sequence, sends the noticed quantities of the extended state observer and the set remark quota to the nonlinear control section, where it compares the error and compensates for the upset. Lastly, the facts accompanying rectification are shipped to the reserved object, and the act of control is reinforced in this manner [46]. The ADRC is mostly composed of the decided transition process (tracking differentiator TD), the extended state observer (ESO), and the nonlinear state error feedback control law (NLSEF). Its typical block is displayed in Figure 3.

PMSMs are generally utilized in great performance drive systems due to their great efficiency, great power density, and fast dynamic response. However, PMSM drives are often affected by various uncertainties such as factor variations, load torque disturbances, inverter nonlinearities, and unmodeled dynamics [47][48]. These disturbances can degrade the performance of conventional control strategies, including MPC. To improve robustness and disturbance rejection capability, ADRC can be integrated with MPC, forming an ADR-MPC strategy. ADR-MPC combines the predictive optimization capability of MPC with the disturbance estimation and compensation ability of ADRC. In this approach, disturbances are appraised in real time utilizing an ESO and then compensated within the predictive control framework.

As demonstrated in Figure 3, v_t^* is the likely orientation recommendation, v_1 to v_n display the reference recommendation signal, z_2 to z_{n+1} Depict the state observation response. Also, z_1 is the disturbance signal response profit of the controlled whole noticed for one extended state observer, and e_1 to e_n demonstrate the error between two points, the recommendation remark value and the state note response value. The tracking differentiator primarily distinguishes the value of the recommendation remark and organizes it appropriately to produce a smoother recommendation at the subsequent level [49]. The comprehensive state observer mainly monitors the disturbed indication and adjusts the necessary control quantity. Since the response size of its gain is determined by extending the observed indication, the accuracy of the numerical model does not need to be expensive. The nonlinear response control regulation effectively compensates for the error indication to achieve improved dynamic performance [50].

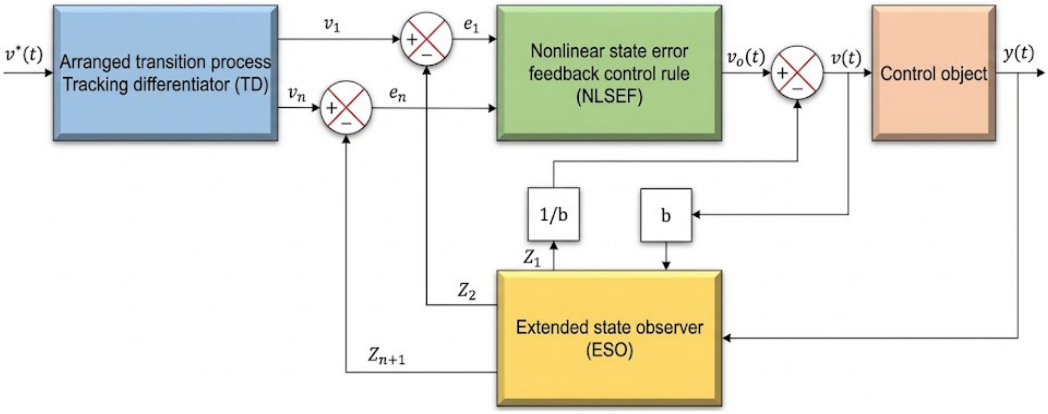

Figure 3. Typical block diagram of n-order ADRC

2.6.2. Speed Loop Control of ADRC

By connecting the torque equation in the mathematical model of a PMSM with the engine motion equation, it can derive the speed equation, which is proved as follows:

$$\dot{\omega} = \frac{3 * i_q * p * \varphi_f}{2J} - \frac{B}{J}\omega - \frac{T_L}{J} \tag{29}$$

where $F_{(\omega)} = -\frac{B}{J}\omega$, $b_0 = \frac{3*p*\varphi_f}{2J}$, $\gamma_{s(t)} = -\frac{T_L}{J}$

Result,

$$\dot{\omega} = F_{(\omega)} + i_q * b_0 + \gamma_{s(t)} \quad (30)$$

In the same recipe, $\gamma_{s(t)}$ may be judged as a plan upset. To couple the ADRC with the speed model, $\gamma_{s(t)}$ May be interchanged with a nonlinear function. In the speed loop antagonistic-commotion boss, the TD and the ESO are expressed as follows:

$$\begin{cases} E_{s0} = \dot{\omega} - v_{s1} \\ \dot{v_{s1}} = -r_{s0}\, fal(E_{s0}, \alpha_{s0}, \delta_{s0}) \end{cases} \quad (31)$$

In the duplicate recipe, E_{s0} depicts the mistake between the speed citation profit and the characteristic indication of the TD itself. This profit is secondhand as the non-denoting function recommendation matches the characteristic indication, and the speed indication is traced by regulating the gain cooperatively fairly. r_{s0} demonstrations the adaptation gain profit of the not denoting function in the characteristic indication of the TD of the speed loop ADRC.

$$\begin{cases} E_{s1} = z_{s1} - \omega \\ \dot{z_{s1}} = z_{s2} - \beta_{s1}\, fal(E_{s1}, \alpha_{s1}, \delta_{s1}) + Fs_{(z_{s1})} + i_q^* * b_0 \\ \dot{z_{s2}} = -\beta_{s2}\, fal(E_{s1}, \alpha_{s1}, \delta_{s1}) \end{cases} \quad (32)$$

similarly, E_{s1} is an error between the speed signal supposed for one lengthened spectator and the speed indication returned, β_{s1} and β_{s2} The gain cooperative is equivalent to the characteristic component of the pursuing indication, and the gain cooperative of the upset wrong guess, individually, the module of differentiator and the lengthened state spectator of the speed loop ADRC are demonstrated in Figure 4 and Figure 5, respectively.

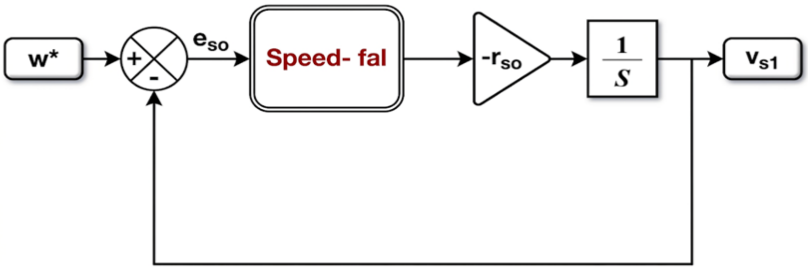

Figure 4. Demonstration illustration of TD

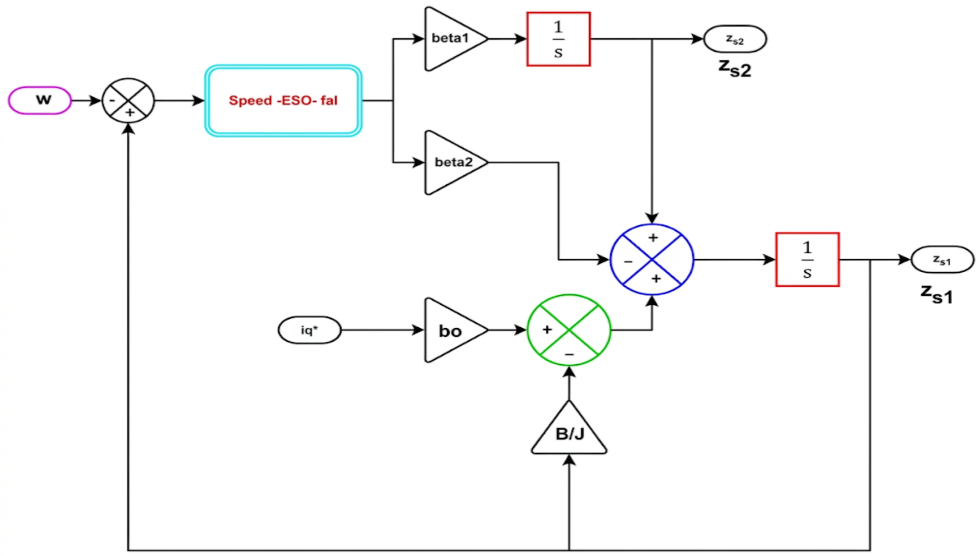

Figure 5. Demonstration illustration of ESO

However, in the speed loop equating, (z_{s2}+fs (z_{s1}))/ b_0 It is used as a part of the control system. In the speed loop, the mechanism standard equating is expressed as follows.

$$\begin{cases} E_{s2} = v_{s1} - z_{s1} \\ i_{qo(t)} = k_s * e_{s2} \\ i^*_{q(t)} = i_{qo(t)} - \dfrac{z_{s2} + Fs(z_{s1})}{b_0} \end{cases} \tag{33}$$

where,k_s is the gain coefficient of the mechanism society; e_{s2} Is the mistake between the pursuing indication of the TD, b_0 Is the repayment determinant of the commotion belief response of the ESO, Furthermore, the speed loop antagonistic-commotion control is displayed in Figure 6. By including disturbance estimates, the predictive model becomes more accurate and robust. A larger bandwidth results in faster disturbance estimation but may amplify measurement noise.

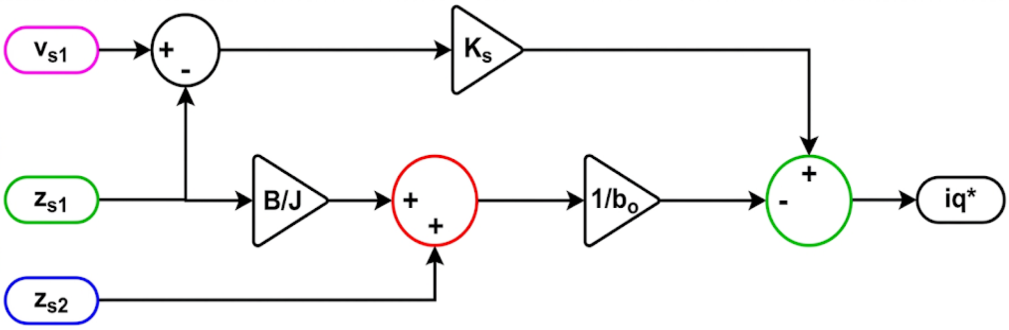

Figure 6. Speed loop control based on the ADRC method

2.6.3. Cost Function of ADRC-MPC

The control architecture in Figure 7 illustrates a detailed integrated hierarchical mechanism for a 6-phase PMSM with speed control by the ADRC and current control by FCS-MPC. In the outer loop, the ADRC scheme relies on the LESO to estimate disturbances and unmodeled dynamics of the system continuously, which allows for disturbance compensation and robustness enhancement. The speed regulator outputs the reference control signal that is then carried over to the inner loop for current control using FCS-MPC. Here, the model of a VSI in the α-β subspace is used in discrete time, and a cost function is defined to compare every switching state and choose the one that achieves the best current tracking. This chosen switching state is then applied through the PWM modulator driving the six-phase inverter.

Additionally, the present system uses Clarke and Park conversions to change the phase currents measured into $\alpha - \beta$ and dq reference frames, thus allowing independent control of the torque and flux components, respectively. Furthermore, rotor position feedback from an encoder/resolver helps the system to synchronize control variables accurately. Moreover, the adoption of this hybrid ADRC-MPC setup leads to an improvement in the dynamic reaction, disturbance rejection, and accuracy of control, which makes it suitable for high-performance multi-phase motor drive applications. The objective function is utilized to select the best voltage vector. A typical cost function is written as follows:

$$g = (i^*_d - i_d(k+1))^2 + (i^*_q - i_q(k+1))^2 \tag{34}$$

where i^*_d, i^*_q , are reference currents.

For a better understanding of the implementation procedure, the overall flowchart of the suggested ADRC-MPC control scheme is plotted in Figure 8. The control process starts by initializing the motor and controller parameters and then proceeds to measure the six-phase currents, motor speed, and rotor position. The currents measured are fed into subspaces d−q and x−y, which correspond to the torque-producing and non-torque-producing components, respectively. The lumped disturbance is estimated by LESO and compensated by the ADRC speed-control loop to produce the desired current references. Then, the MPC uses the discrete-time predictive model and cost function to choose the candidate inverter switching states. This switching state is determined to be the one that reduces the control objective to a minimum and is applied to the six-phase inverter. This collocated arrangement allows ADRC to improve the rejection of disturbances and MPC to regulate the current quickly and suppress unwanted x−y current components.

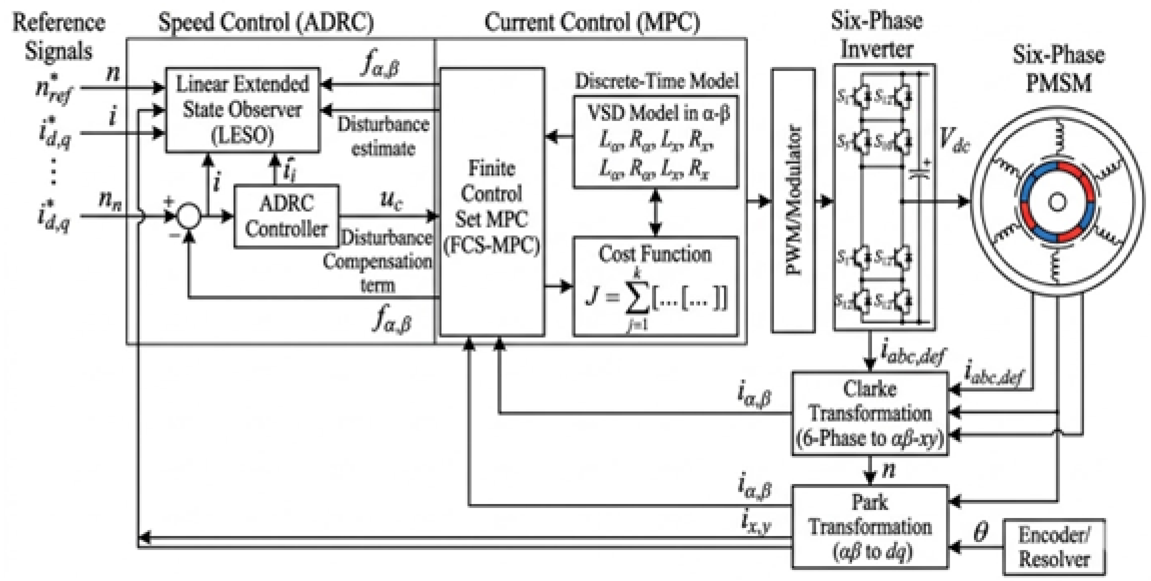

Figure 7. Proposed ADRC-MPC strategy

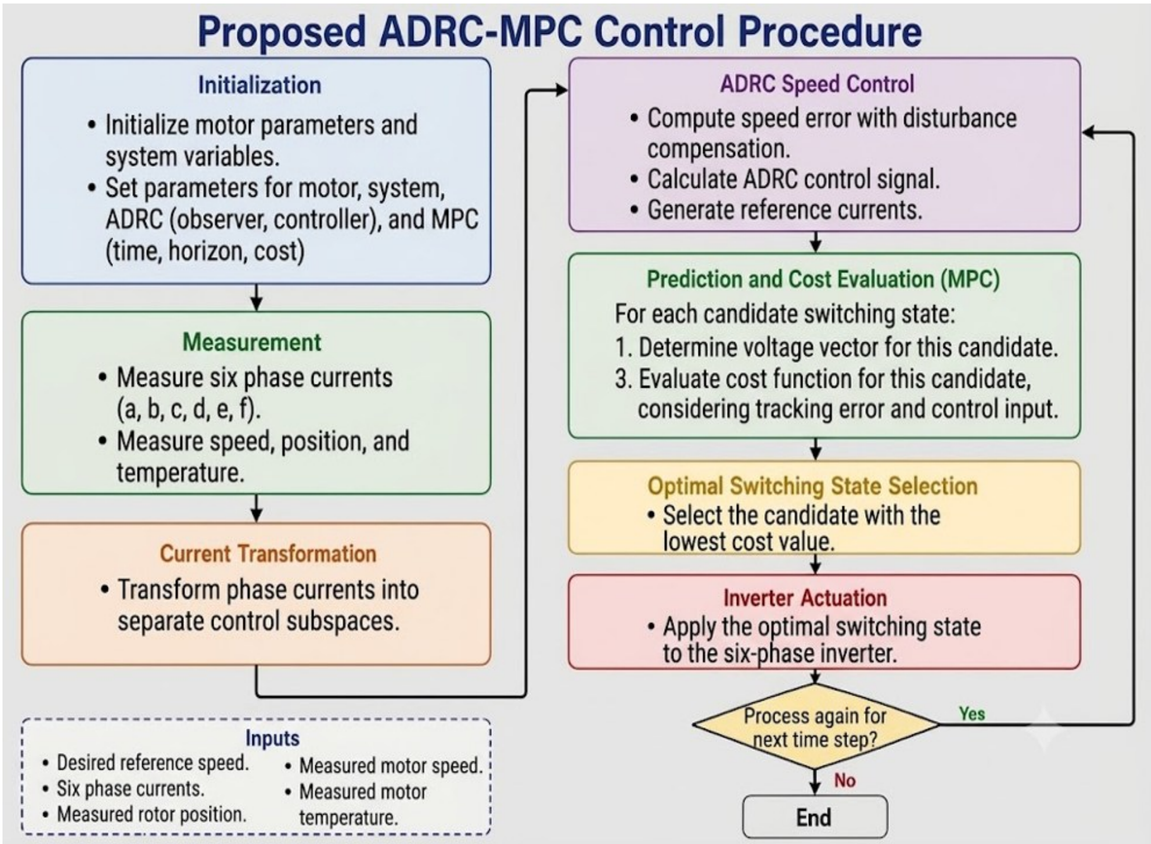

Figure 8. Flowchart of the proposed ADRC-MPC control procedure for the 6-phase PMSM

2.7. ADRC Parameter Tuning Procedure

The bandwidth-parameterization approach tunes the ADRC parameters, providing a systematic way to adjust them without requiring independent trial and error for multiple controller gains. The controller bandwidth ωc is first determined based on the desired speed-loop dynamic response, but is not too high compared to the inner current-control bandwidth. This bandwidth, ω_o, of LESO is then chosen to be larger than ωc to achieve a sufficiently fast estimation of the lumped disturbances while still keeping the measurement noise small. It is assumed that in this study, ωc = 250 rad/s and ωo = 2000 rad/s, with the ratio of bandwidths ($\omega o/\omega c$) being equal to 8. The LESO gains are parameterized by using the selected observer bandwidth, based on the observer characteristic polynomial. This bandwidth-based technique yields a reproducible balance among disturbance-estimation speed, closed-loop dynamic response, and noise sensitivity.

2.8. MPC Weighting-Factor Selection

The weighting factor λxy determines the relative importance assigned to the suppression of non-torque-producing $x - y$ currents in the MPC cost function. A small λxy prioritizes $d - q$ current tracking but may permit larger harmonic-subspace currents, whereas an excessively large value may improve $x - y$ current suppression at the expense of transient tracking performance. Therefore, λxy is selected through a sensitivity-based tuning procedure by progressively increasing its value and evaluating the resulting d–q tracking error, $x - y$ current magnitude, and current THD under identical operating conditions. The final value is chosen as the smallest weighting factor that provides satisfactory $x - y$ current suppression without a noticeable deterioration in torque-producing current tracking. Find the value of λxy by using the trial-and-error approach. The value of the correlation coefficient, λxy, is 0.56.

2.9. Design of ADRC strategy

Every sample instant, the proposed FCS-MPC considers the finite number of admissible inverter switching states. The voltage vector for every candidate state is computed, the $d - q$ and $x - y$ currents are forecasted based on the machine model (discrete-time), and the value of the cost function is determined. The switching state that results in the least cost is then applied to the inverter. The ADRC unit also needs to provide real-time updates of the state of LESO and calculations of disturbance compensation. The algorithm does not need to optimize the model numerically, unlike the conventional MPC, because the prediction horizon is one-step, but this adds extra arithmetic operations. The computational complexity is thus still deterministic and can be implemented in real time as long as the maximum execution time of the algorithm is less than the desired sampling period.

3. RESULTS AND DISCUSSION

To validate the proposed control strategy, MATLAB/Simulink has been used. The parameters of the used PMSM motor and the solver settings alongside the particular tuning gains are listed in Table 1 and Table 2, respectively. The system is modeled and tested under different scenarios to ensure optimal performance and maintain accuracy control.

Table 1. Parameters of 6-Phase PMSM.

Parameter	Value	Unit
Tn	15	Nm
N	1000	rpm
Rs	0.45	Ω
Ld	4.5	mH
Lq	4.5	mH
Φ	0.125	Wb
P	4	
J	0.0048	$Kg.m^2$

Table 2. Solver settings and the specific tuning gains for the ADRC-MPC

Control Parameter	Symbol	Value	Unit
DC-link voltage	Vdc	540	V
Sampling time	Ts	100	µs
Prediction horizon	Np	1	step
LESO observer bandwidth	ω_o	2000	rad/s
ADRC controller bandwidth	ω_C	250	rad/s

Figure 9 illustrates the conventional and proposed methods' responses at a non-uniform switching frequency of 14.2 kHz, which is often characterized by spread-spectrum harmonic noise and higher switching losses due to the stochastic nature of finite-control-set vector selection. By comparison, the disturbance-rejection-enhanced, ripple-reduced ADRC-MPC exhibits a lower average switching frequency of 10.8 kHz.

This yields a savings of about 24%, and the observer-based method not only improves the existing quality but also increases the efficiency of the six-phase inverter by diminishing unnecessary switching transitions. The current response of the E-phase at different torque steps (0, 10, and 15 N m), using simulation, suggests that there is a significant difference in the performance of the two control approaches.

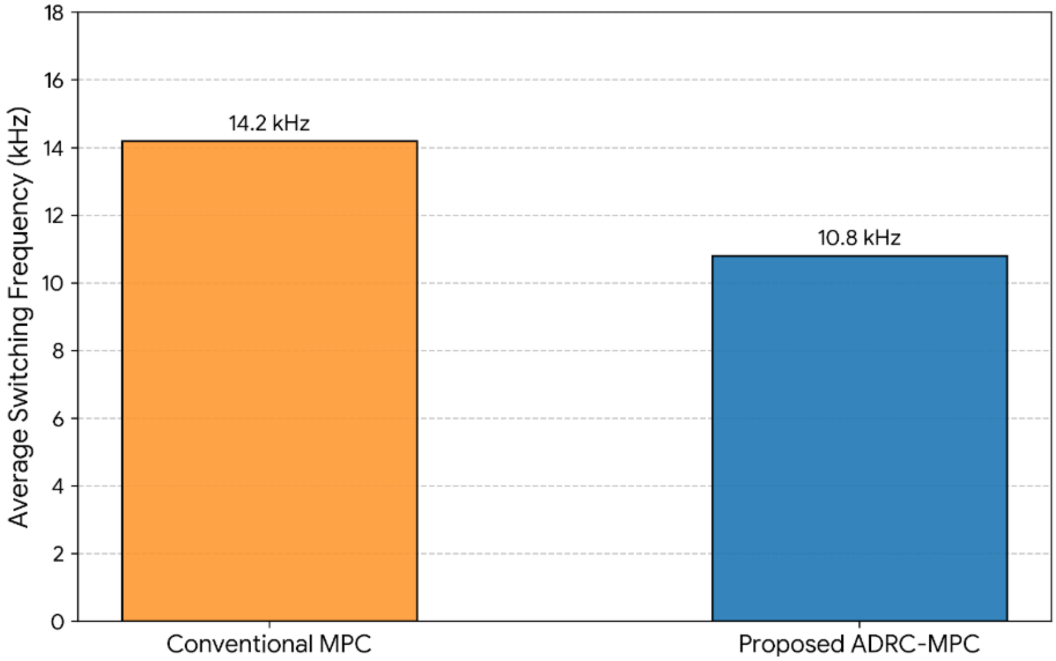

Figure 9. Switching frequency of the classical MPC and the proposed method

Figure 10 demonstrates that the conventional MPC has a high noise floor and considerably high current ripple, both at zero load and during transient steps. The consequence of this distortion is a relatively high Total Harmonic Distortion (THD) of 7.6%, which can be attributed to the absence of integral action and the unresponsiveness to unmodeled dynamics. As shown, the proposed ADRC-MPC is capable of generating a far cleaner and more sinusoidal current waveform. The proposed solution, which uses an observer to estimate and reject distortions in real-time, achieves a THD of 2.3, providing smoother operation and increased efficiency of the 6-phase PMSM drive. The switching of the torque steps in the ADRC-MPC also happens much quicker and more stably, and the overshoot is very minimal as compared to the traditional method.

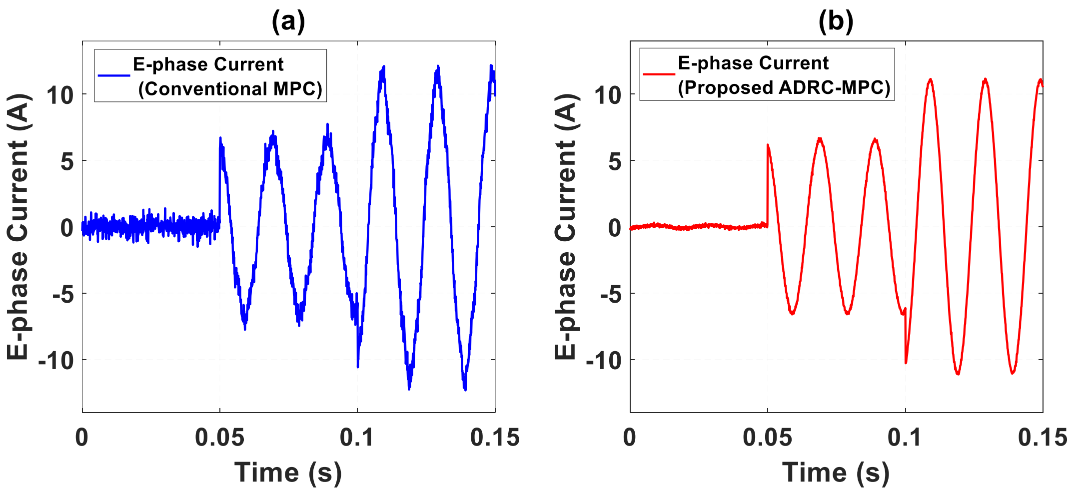

Figure 10. Current response of the E-phase

Figure 11 shows the comparative response of the two control methodologies in terms of torque responses. As observed, the proposed ADRC-MPC strategy is better in terms of dynamic performance. The conventional MPC reaction to the torque steps of 0.05s 10 Nm and 0.1s 15 Nm has a large overshoot and long oscillations. The fact that this effect forms a ringing demonstrates that this method is vulnerable to unmodeled dynamics and that it does not have a strong compensation mechanism. Thus, the ADRC-MPC attains a significantly quicker, smoother, and near-overshoot free rising to the reference torque. The constant Torrance ripple is also significantly less in the proposed approach, giving an even-handed mechanical production. These findings support the notion that the addition of an active disturbance rejection observer enables the controller to cancel lumped disturbances in real-time, which alone yields high-precision torque tracking, which cannot be accomplished by conventional MPC.

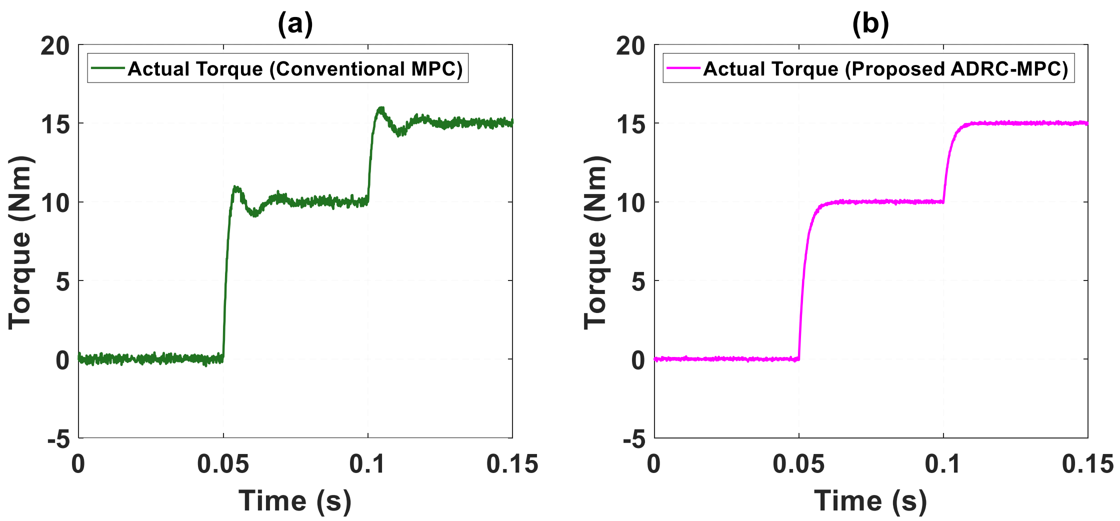

Figure 11. Indicates the MPC response to the torque

The torque tracking error of both controllers is shown in Figure 12. Conventional MPC keeps the error very small near zero during steady-state operation, but very large spikes in the error, reaching up to ± 0.45 Nm, are observed at the load's transitions at 0.05 s and 0.10 s. The proposed ADRC-MPC, on the other hand, achieves a transient error less than ±0.1 Nm, and the error quickly goes to zero following each disturbance. The torque error is much smaller, which shows that the controller can more accurately track the target value in different operating conditions and is more robust.

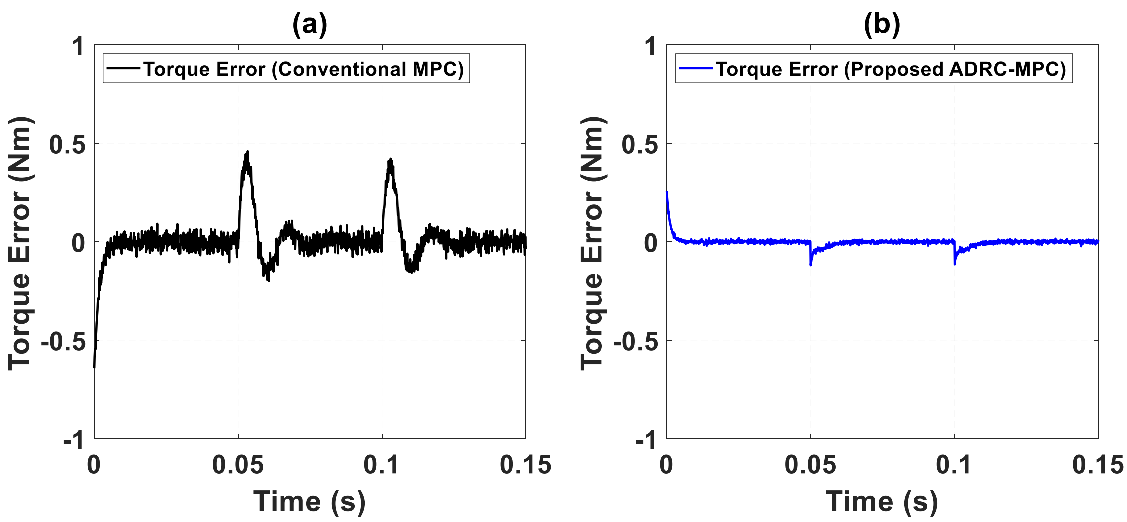

Figure 12. Error in the PMSM torque

The responses of the rotor speed for the two control methods are depicted in Figure 13. The reference speed is kept constant at 1000 rpm for the whole simulation. The response time of both controllers is around 0.02 s to reach the reference speed from standstill. With load disturbances at 0.05 s and 0.10 s, however, the conventional MPC suffers from perceptible speed dips of 40-60 rpm, which in turn recover. The proposed ADRC-MPC, on the other hand, keeps the speed close to 1000 rpm with only small deviations around 10 rpm. The results demonstrate that the ADRC-based predictive controller has great disturbance rejection capability and good speed regulation.

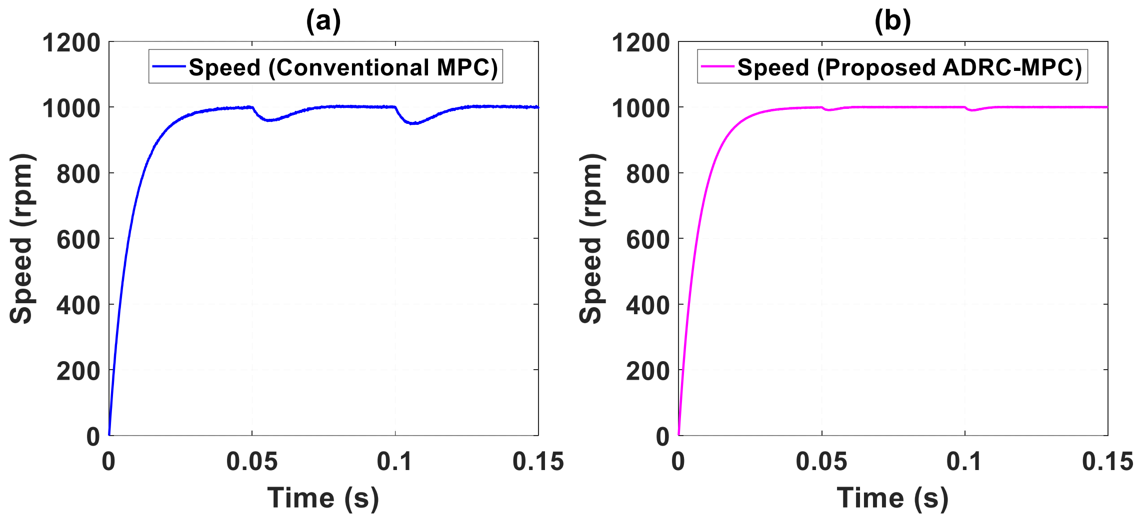

Figure 13. Motor's speed response

The speed tracking error is shown in Figure 14. The typical MPC suffers from large transients of around -140 rpm at 0.05 s and +125 rpm at 0.10 s, and slowly decays to zero. In contrast, ADRC-MPC causes the speed error to be bound within about -30 rpm, and the convergence is much greater after encountering each disturbance. The difference in speed error shows that the proposed controller has good dynamic regulation, and it can reject external load changes.

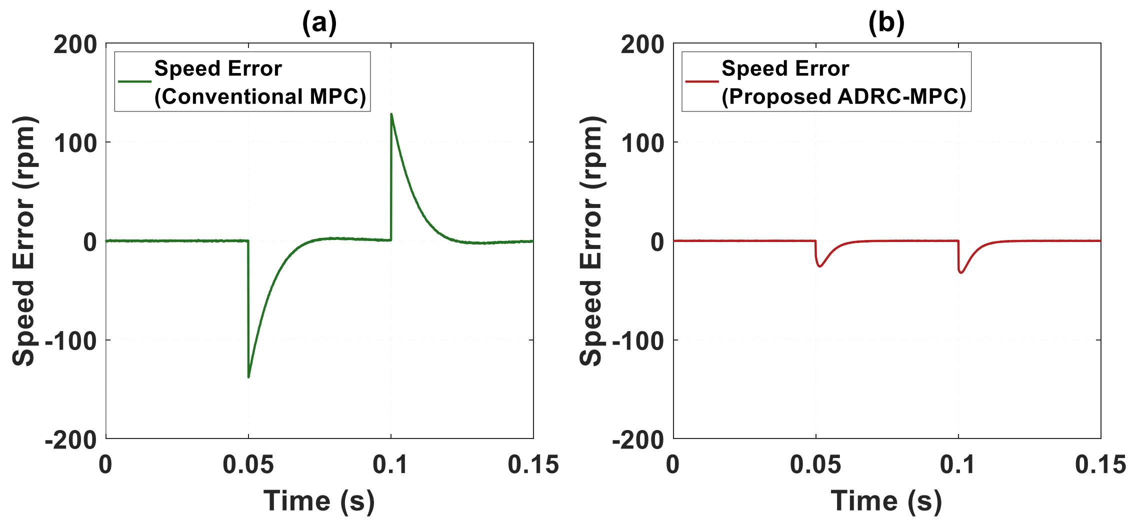

Figure 14. Speed error of the motor.

The q-axis current response, which is dependable for torque production, is shown in Figure 15. At 0.05 s, the current is about 20 A (the 10 Nm torque demand), and at 0.10 s, it is about 30 A (the 15 Nm torque demand). MPC shows significant ripple and oscillatory behaviour around the reference values in the conventional MPC.

Vol. 8, No. 4, August 2026, pp. 1236-1258

The proposed ADRC-MPC, on the contrary, has a smaller steady-state ripple of the current, which shows better current regulation and more efficient torque generation.

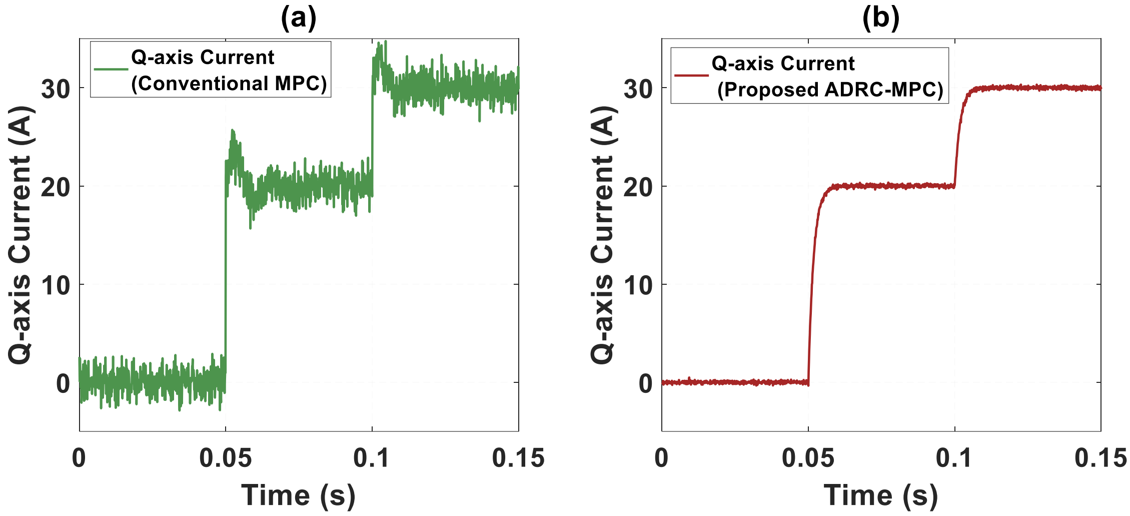

Figure 15. Q-axis current response

The d-axis current under both of these control methods is compared in Figure 16. The ideal is id=0, which means the control should be zero current. The MPC of the conventional MPC has a fluctuation of about −0.5 A to 0.2 A, especially at transient intervals. On the other hand, when the proposed ADRC-MPC is used, the holding current of the d-axis is very close to zero, and the current fluctuation is only a few tens of nanoamperes. This not only reduces the unnecessary additional current flowing through the coil to magnetize the motor, but also increases the efficiency and keeps the produced torque optimal.

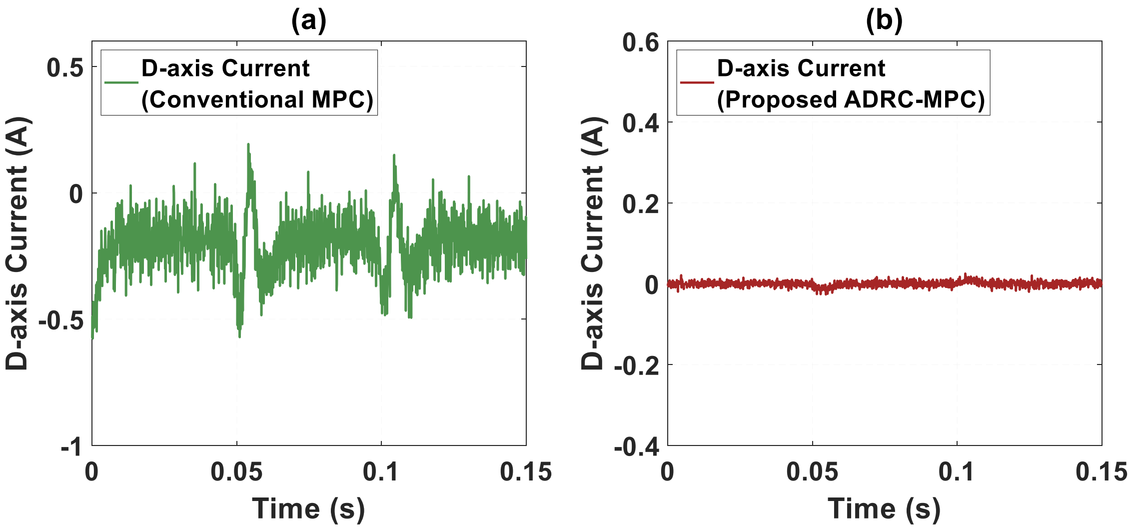

Figure 16. D-axis current response

The x-axis harmonic current for both control strategies is shown in Figure 17. In the conventional MPC, the harmonic currents level up to ~ ±8 mA, particularly for load transition times, around 0.05 s and 0.10 s. On the contrary, the proposed ADRC-MPC has almost completely suppressed these harmonic components and kept the harmonic current within ±0.5 mA during the simulation. This is a significant reduction in harmonic current, reflecting the usefulness of the suggested controller in suppressing the secondary subspace currents that lead to additional copper losses, minimizing torque ripple, and enhancing the efficiency of the six-phase PMSM.

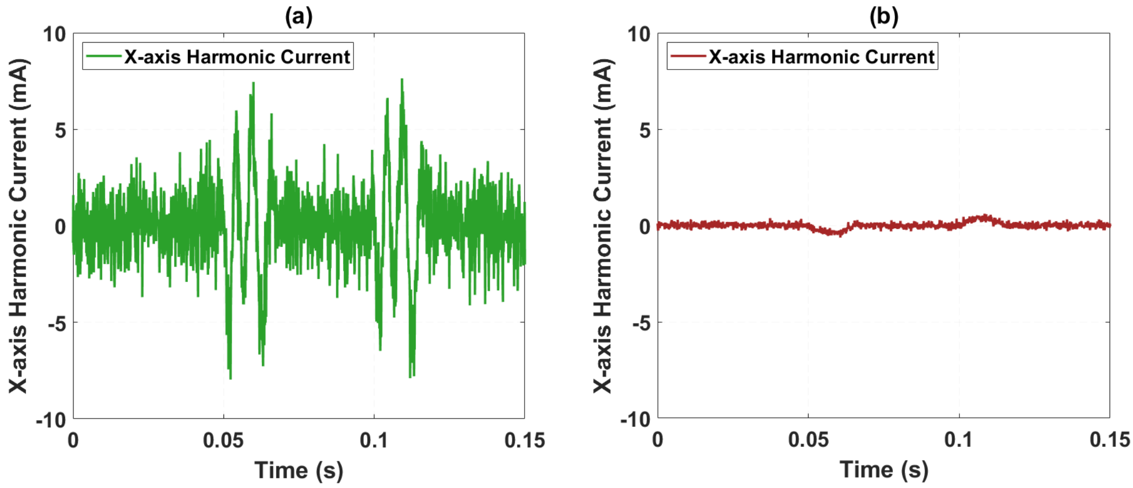

Figure 17. X-axis harmonic current response

Table 3 offers a detailed comparison of the standard MPC and the suggested ADRC-MPC strategy, both quantitatively and qualitatively. Apart from the substantial drop in the current THD, speed deviation, recovery time, torque error, torque ripple, and switching frequency, the proposed controller is shown to regulate the d−q current components. As a result, the d-axis current is closer to its reference with less transient deviation, and the q-axis current has a faster and smoother response to loading changes, leading to better torque response. In addition, the cancellation of the non-torque-producing x−y current components is evidence of the superior harmonic-current regulation performance of the suggested predictive current control strategy. In general, the overall improvements validate that the proposed ADRC-MPC improves the dynamic response, current regulation, harmonic suppression, and disturbance rejection for the simulation conditions under investigation.

Table 3. Compare the performance of the suggested ADRC-MPC with the conventional MPC

Performance Index	Conventional MPC	Proposed ADRC-MPC	Improvement
Average Switching Frequency	14.2 kHz	10.8 kHz	23.9% reduction
Speed Tracking	Good	Excellent	Faster convergence
Speed Deviation under Load	≈ 50 rpm	< 10 rpm	≈ 80% lower
Maximum Speed Error	≈ 140 rpm	≈ 30 rpm	≈ 78.6% reduction
Torque Overshoot	≈ 1 Nm	Nearly 0 Nm	Almost eliminated
Maximum Torque Error	≈ 0.45 Nm	< 0.10 Nm	≈ 77.8% reduction
Torque Ripple	High	Very Low	Significantly reduced
Phase Current Ripple	Noticeable	Very Small	Improved waveform quality
Q-axis Current Ripple	High	Low	Improved current tracking
D-axis Current Deviation	± 0.5 A	± 0.02 A	≈ 96% reduction
X-axis Harmonic Current	± 8 mA	± 0.5 mA	≈ 93.8% reduction
Dynamic Response	Moderate	Excellent	Faster transient response
Disturbance Rejection	Moderate	Excellent	Strong robustness
Steady-State Accuracy	Good	Excellent	Higher precision
Switching Losses	High	Low	Reduced inverter losses
Overall Efficiency	Moderate	High	Improved system efficiency

A comparison of the proposed ADRC-MPC strategy with the representative control approaches found in the literature is made qualitatively in Table 4. The approach of [9], based on the ADRC controller, has a good disturbance rejection property, but there is no specific treatment of the control of the non-torque-producing current components in multiphase machines. The robust predictive strategy of [16] has better tolerance to parameter perturbations, while the predictive current-control method of [17] has mainly improved current regulation. In [22], the virtual-voltage-vector predictive method is used for suppressing harmonics in current in the case of a 6-phase PMSM, and it works well, but is dependent on the accuracy of the predictive model and the design of virtual voltage vectors. Explicit current subspace regulation of the d−q current and x−y current is performed in the proposed ADRC-MPC, compared with the active disturbance estimation and compensation in the conventional MPC. Hence, the suggested framework offers a harmonious framework to enhance disturbance rejection, dynamic current tracking, and harmonic-current suppression. However, the comparison made in the present paper is qualitative as the studies cited use different motor parameters and operating conditions, and the proposed strategy needs to be experimentally validated.

Table 4. Provides a qualitative comparison between the suggested ADRC-MPC strategy and typical control schemes found in the literature

Reference	Main Feature	Disturbance Rejection	Harmonic / (x-y) Current Suppression	Model Robustness	Main Limitation
[9]	ADRC with disturbance compensation for PMSM speed regulation	High	Not specifically addressed	High	Mainly focused on speed-loop disturbance rejection rather than multiphase harmonic-subspace regulation.
[16]	Robust predictive control considering parameter perturbations	Good	Moderate	High	Does not explicitly integrate active disturbance rejection with (x-y) subspace regulation
[17]	Improved predictive current regulation for PMSM drives	Moderate	Good	Moderate	Primarily focused on current-control performance
[18]	Direct prediction and optimization of control actions	Moderate	Moderate	Moderate	Performance can deteriorate under model mismatch and external disturbances.
[22]	Robust predictive current control using virtual voltage vectors for six-phase PMSM	Moderate	High	Good	Requires appropriate virtual-vector construction and remains dependent on the predictive machine model
Proposed ADRC-MPC	ADRC-based disturbance estimation combined with predictive (d-q/x-y) current regulation	High	High	High	Requires coordinated ADRC/MPC tuning and further experimental validation

In summary, this detailed comparative study indicates that the proposed ADRC-MPC strategy can outperform the conventional MPC in all considered performance metrics under the same operating conditions. The combination of the Active Disturbance Rejection Control (ADRC) framework and the Model Predictive Control (MPC) effectively improves the dynamic response: the active assessment and rejection of internal uncertainties, external disturbances, and model mismatches in real time.

In terms of speed performance, the proposed controller has not only a faster convergence to the reference speed but also excellent regulation when the load torque suddenly changes. For the conventional MPC, speed variations after disturbances are observed, while the speed variations for ADRC-MPC are effectively suppressed; therefore, the speed error is much smaller after a disturbance, and the transient stability is improved. This excellent disturbance rejection performance allows the drive system to maintain tracking accuracy at high-speed conditions even in the case of rapid variations in operating conditions.

The torque responses are also presented to confirm the usefulness of the suggested approach. The conventional MPC has a significant overshoot at the load transition times of 0.05 s and 0.10 s, generates oscillatory responses, and has relatively large torque tracking errors during the load transition. The proposed ADRC-MPC, however, rapidly follows the commanded torque with a near-zero overshoot and with much less torque ripple. Such action demonstrates the effectiveness of the disturbance observer built into the ADRC structure in compensating for the load disturbance before it enters the predictive control loop, which helps accelerate the electromagnetic torque regulation.

The present regulation has also been substantially improved. The proposed controller produces smooth phase-current waveforms with significantly reduced phase-current ripple and can regulate both the q-axis and d-axis currents. The q-axis current tracks the desired torque demand quite smoothly without any significant oscillations, while the d-axis current stays very close to zero during the entire simulation, meeting the basic requirement and enabling the highest possible torque production efficiency. In addition, the suppression of harmonic currents in the secondary x-axis subspace illustrates the ability of the proposed controller to reduce undesirable current components that cause additional copper losses, electromagnetic vibration, and torque pulsations.

The main benefit of the suggested method is that it improves performance and reduces inverter switching activity. As evident in the comparison of switching frequency, the average switching frequency is diminished to 10.8 kHz with the proposed ADRC-MPC compared to 14.2 kHz of the conventional MPC, which means an approximate 23.9% reduction. This minimizes switching losses, reduces thermal stress on the semiconductor devices, and improves the overall efficiency and reliability of the power converter without compromising on control accuracy or dynamic performance.

In general, the results obtained display that the suggested ADRC-MPC has excellent dynamic performance, steady-state accuracy, disturbance rejection, harmonic suppression, and switching efficiency. The proposed controller shows better performance in terms of current ripple, torque ripple, speed and torque error, current tracking performance, robustness to load disturbances, and low switching frequency compared to the standard MPC. The suggested ADRC-MPC is an appealing and practical control solution for the 6-phase PMSM drive system used in high-performance applications like electric vehicles, aerospace propulsion, renewable energy conversion, and industrial automation, where high reliability, energy efficiency, and rapid dynamic response are required.

4. CONCLUSION AND FUTURE WORK

In this paper, a six-phase PMSM drive with an integrated ADRC-MPC control algorithm was designed, which integrated the disturbance estimation and compensation capability of ADRC with the fast predictive current regulation capability of MPC. The overall theoretical contribution is the coordinated control of the outer speed loop and predictive current loop, which enhances robustness to load disturbances while minimizing the non-torque-producing current components in the non-torque-creating subspace. The performance of the suggested strategy has been compared with standard MPC, and MATLAB/Simulink results showed that the suggested strategy has better dynamic and steady-state performance with a reduction of stator current THD from 7.6% to 2.3%, a reduction of maximum speed dip from 150 rpm to 35 rpm, and a reduction of recovery time from 40 ms to 10 ms under the investigated load disturbances. The lower average switching frequency also suggests reduced switching activity, and the torque tracking and current decoupling capabilities were enhanced. The results from an engineering point of view show the ability of using predictive control combined with active disturbance rejection to improve the robustness and harmonic-current regulation of multiphase PMSM drives. The present study, however, only considers MATLAB/Simulink validation. The suppression of x-y current components was not measured and/or used to calculate switching loss in semiconductors, and the reduction in switching frequency was not measured or used to directly calculate system efficiency; thus, the suppression of x-y current components and the reduction in switching frequency are not direct quantitative measures of improved system efficiency. In addition, the controller needs to be implemented and tested on a 6-phase PMSM platform. The future work will be dedicated to Hardware-in-the-Loop validation, real-time implementation on a DSP-FPGA, experimental efficiency and thermal-loss evaluation, and analysis for further open-phase and other fault conditions for fault-tolerant multiphase drive applications.

Conflicts of Interest

The authors have no conflict of interest to declare.

REFERENCES

[1] M. A. Mossa, A. S. Al-Sumaiti, T. Duc Do, A. Iqbal, and H. Echeikh, “A Novel Sensorless Control for Multiphase Induction Motor Drives Based on Singularly Perturbed Sliding Mode Observer-Experimental Validation,” *Applied Sciences*, vol. 10, no. 8, p. 2776, Apr. 2020, https://doi.org/10.3390/app10082776.

[2] Z. H. Saleh, “Enhanced Dynamic Control of Quadcopter PMSMs Using an ILQR-PCC System for Improved Stability and Reduced Torque Ripples”, *Journal of Robotics and Control (JRC)*, vol. 5, no. 6, pp. 1652–1663, Sep. 2024. https://doi.org/10.18196/jrc.v5i6.23159.

[3] M. S. Rafaq and J. W. Jung, “A Comprehensive Review of State-of-the-Art Parameter Estimation Techniques for Permanent Magnet Synchronous Motors in Wide Speed Range,” *IEEE Trans. Ind. Informatics*, vol. 16, no. 7, pp. 4747–4758, 2020, https://doi.org/10.1109/TII.2019.2944413.

[4] P. Q. Khanh, H. P. H. Anh, and C. M. Thuyen, “Improving PMSM Control Based on Optimizing the Output Membership Function of Fuzzy PI Controller with Weighted Modified Jaya Algorithm”, *Journal of Robotics and Control (JRC)*, vol. 6, no. 4, pp. 1938–1948, Jul. 2025. https://doi.org/10.18196/jrc.v6i4.27080.

[5] A. H. Levent, A. Lordoglu, and M. G. Aydeniz, “Design and Optimization of Permanent Magnet Synchronous Motor for Electric Vehicle Applications,” in P*roceedings - 2020 IEEE 2nd Global Power, Energy and Communication Conference, GPECOM*, pp. 148–151, Oct. 2020, https://doi.org/10.1109/GPECOM49333.2020.9247885.

[6] A. Hezzi, M. N. Abdelkrim and S. B. Elghali, "Sensorless Backstepping Drive for a Five-Phase PMSM based on Unknown Input Observer," *2020 20th International Conference on Sciences and Techniques of Automatic Control and Computer Engineering (STA)*, pp. 125-130, 2020, https://doi.org/10.1109/sta50679.2020.9329327.

[7] Z. Wang, T. W. Ching, S. Huang, H. Wang, and T. Xu, “Challenges Faced by Electric Vehicle Motors and Their Solutions,” *IEEE Access*, vol. 9, pp. 5228–5249, 2021, https://doi.org/10.1109/ACCESS.2020.3045716.

[8] M. Kim, Y. Bae, S. Jun, S. Hwang, K. Lee, and H. Li, "Switch Open Fault Detection of Asymmetric 6-phase PMSM Based on Normalized Stationary Reference Frame dq-axis Currents," *2024 IEEE Energy Conversion Congress and Exposition (ECCE)*, pp. 5516-5522, 2024, https://doi.org/10.1109/ECCE55643.2024.10861008.

[9] T. Deng, Z. Su, J. Li, P. Tang, X. Chen, and P. Liu, "Advanced Angle Field Weakening Control Strategy of Permanent Magnet Synchronous Motor," *IEEE Transactions on Vehicular Technology*, vol. 68, no. 4, pp. 3424–3435, Apr. 2019, https://doi.org/10.1109/TVT.2019.2901275.

[10] Y. Wu *et al*., "Hierarchical predictive control for electric vehicles with hybrid energy storage system under vehicle-following scenarios," *Energy*, vol. 251, p. 123774, Jul. 2022, https://doi.org/10.1016/j.energy.2022.123774.

[11] T. T. Pham and N. T. Pham, "A Hybrid PI–SOSM Control Strategy with Disturbance Observer for Enhanced Dynamic Response of IM Drives," *Buletin Ilmiah Sarjana Teknik Elektro*, vol. 7, no. 4, pp. 702–714, Oct. 2025, https://doi.org/10.12928/biste.v7i4.14458.

[12] X. Wang *et al*., "Torque Ripple Reduction in Sectored Multi-Three-Phase Machines Based on PWM Carrier Phase Shift," in *IEEE Transactions on Industrial Electronics*, vol. 67, no. 6, pp. 4315-4325, June 2020, https://doi.org/10.1109/TIE.2019.2931239.

[13] R. K. Chillab and H. A. Hasan, "Adaptive Hybrid Fuzzy–Neural PID Control of Speed Regulation and Torque Ripple Reduction of BLDC Motors," *Buletin Ilmiah Sarjana Teknik Elektro*, vol. 8, no. 3, pp. 792–810, Jun. 2026, https://doi.org/10.12928/biste.v8i3.16182.

[14] Saif Talal Bahar and Raed A. Abd-Alhmeed, "Reduce-Complexity of Predictive Current Control for a 3-Phase Voltage Source Inverter," *Journal of Techniques*, vol. 7, no. 3, pp. 16–25, Sep. 2025. https://doi.org/10.51173/jt.v7i3.2621.

[15] Q. H. Le and N. T. Pham, "Predefined-Time Super-Twisting Disturbance-Observer-Based Speed Control for PI-Based FOC Induction Motor Drives," *Buletin Ilmiah Sarjana Teknik Elektro*, vol. 8, no. 2, pp. 451–462, Apr. 2026, https://doi.org/10.12928/biste.v8i2.15761.

[16] L. Yan *et al*., "Suppression of Major Current Harmonics for Dual Three-Phase PMSMs by Virtual Multi Three-Phase Systems," in *IEEE Transactions on Industrial Electronics*, vol. 69, no. 6, pp. 5478-5490, June 2022, https://doi.org/10.1109/TIE.2021.3091922.

[17] Z. Zhu, S. Wang, B. Shao, L. Yan, P. Xu, and Y. Ren, "Advances in dual-three-phase permanent magnet synchronous machines and control techniques," *Energies*, vol. 14, no. 22, p. 7508, 2021, https://doi.org/10.3390/en14227508.

[18] M. K. Ismael, S. T. Bahar, and A. A. Abdullah, "Harmonic elimination method for permanent magnet synchronous motor utilizing active disturbance rejection control," *Proc. Eng. Technol. Innov.*, vol. 30, pp. 11–23, Jun. 2025,, https://doi.org/10.46604/peti.2024.14386.

[19] M. A. Mossa, H. Echeikh, A. A. Z. Diab, H. Haes Alhelou, and P. Siano, "Comparative Study of Hysteresis Controller, Resonant Controller and Direct Torque Control of Five-Phase IM under Open-Phase Fault Operation," *Energies*, vol. 14, no. 5, p. 1317, Feb. 2021, https://doi.org/10.3390/en14051317.

[20] H. Chen, Q. Gao, T. Yang, and M. Sumner, "Fundamental PWM Excitation Based Rotor Position Estimation for a Dual Three-Phase Permanent Magnet Synchronous Machine," *IEEE Journal of Emerging and Selected Topics in Industrial Electronics*, vol. 4, no. 2, pp. 659–668, Apr. 2023, https://doi.org/10.1109/jestie.2022.3223880.

[21] H. Wang, X. Zheng, X. Yuan, and X. Wu, "Low-Complexity Model-Predictive Control for a Nine-Phase Open-End Winding PMSM With Dead-Time Compensation," in *IEEE Transactions on Power Electronics*, vol. 37, no. 8, pp. 8895-8908, Aug. 2022, https://doi.org/10.1109/TPEL.2022.3146644.

[22] M. Yao, J. Peng, and X. Sun, "Robust model predictive current control for six-phase PMSMs with virtual voltage vectors," *J. Power Electron*., vol. 22, pp. 1885–1896, 2022, https://doi.org/10.1007/s43236-022-00496-w.

[23] Y. Hu, Y. Li, X. Ma, X. Li, and S. Huang, "Flux-Weakening Control of Dual Three-Phase PMSM Based on Vector Space Decomposition Control," *IEEE Transactions on Power Electronics*, vol. 36, no. 7, pp. 8428–8438, July 2021, https://doi.org/10.1109/tpel.2020.3044574.

[24] S. Talal Bahar, H. Qiu, D. Rahman Neama, F. Fawzi Hashim, and H. Yasseen, "An Improved Cost Function Based on Model Predictive Current Control for Five-Phase PMSM," *Edison Journal for electrical and electronics engineering*, vol. 3, no. 1, pp. 32–38, Oct. 2025. https://doi.org/10.62909/ejeee.2025.004.

[25] K. Yu, Z. Wang, M. Gu, and X. Wang, "Universal Control Scheme of Dual Three-Phase PMSM Drives With Single Open-Phase Fault," in *IEEE Transactions on Power Electronics*, vol. 37, no. 12, pp. 14034-14039, Dec. 2022, https://doi.org/10.1109/TPEL.2022.3195526.

[26] Q. Wei, C. Tan, M. Hao, X. Chen, Y. Li, and W. Ge, "Model-free predictive current control based on improved sliding mode disturbance observer," *Transactions of the Institute of Measurement and Control*, vol. 46, no. 13, pp. 2593–2602, Mar. 2024, https://doi.org/10.1177/01423312241233315.

[27] S. T. Bahar, W. Wang, and H. Qiu, "AI-Enhanced Model Predictive and Active Disturbance Rejection Control for High-Performance Permanent Magnet Synchronous Motor Drives," *Energies*, vol. 19, no. 11, p. 2574, May 2026, https://doi.org/10.3390/en19112574.

[28] W. Zhou, Y. Guo, X. Xiao, Z. Song and Z. Liu, "Model Predictive Current Control of PMSM Based on a Novel Sliding Mode Disturbance Observer," *2024 IEEE 6th Advanced Information Management, Communications, Electronic and Automation Control Conference (IMCEC)*, pp. 464-469, 2024, https://doi.org/10.1109/IMCEC59810.2024.10575098.

[29] Y. Huang, S. Liu, R. Pang, X. Liu, and X. Rao, "Model Predictive Current Control for Six-Phase PMSM with Steady-State Performance Improvement," *Energies*, vol. 17, no. 21, p. 5273, Oct. 2024, https://doi.org/10.3390/en17215273.
[30] P. P. Das, S. Satpathy, S. Bhattacharya, V. Veliadis, U. Deshpande and B. Bhargava, "Determination of Parameters of Symmetrical Six-Phase Permanent Magnet Synchronous Machines," *2023 IEEE International Electric Machines & Drives Conference (IEMDC)*, pp. 1-7, 2023, https://doi.org/10.1109/IEMDC55163.2023.10238906.
[31] S. T. Bahar and R. Ghanem Omar, "Permanent Magnet Synchronous Motor Torque Ripple Reduction Using Predictive Torque Control," *Journal of Engineering and Sustainable Development*, vol. 27, no. 3, pp. 394–406, May 2023, https://doi.org/10.31272/jeasd.27.3.9.
[32] W. Taha, P. Azer, A. Poorfakhraei, S. Dhale, and A. Emadi, "Comprehensive Analysis and Evaluation of DC-Link Voltage and Current Ripples in Symmetric and Asymmetric Two-Level Six-Phase Voltage Source Inverters," *IEEE Transactions on Power Electronics*, vol. 38, no. 2, pp. 2215–2229, Feb. 2023, https://doi.org/10.1109/tpel.2022.3214096.
[33] P. P. Das, S. Satpathy, S. Bhattacharya, and V. Veliadis, "Generalized Control Technique for Three-Level Inverter Fed Six-Phase Permanent Magnet Synchronous Machines Under Fault Conditions," in *2022 IEEE Energy Conversion Congress and Exposition (ECCE)*, pp. 1–8, 2022, https://doi.org/10.1109/ecce50734.2022.9947672.
[34] Z. Su, X. Sun, G. Lei, and M. Yao, "Model-Free Predictive Current Control for Dual Three-Phase PMSM Drives With an Optimal Modulation Pattern," *IEEE Transactions on Industrial Electronics*, vol. 71, no. 9, pp. 10140–10149, Sept. 2024, https://doi.org/10.1109/tie.2023.3327554.
[35] Q. Geng, Q. Liu, and W. Zheng, "Weightless Model Predictive Control for Permanent Magnet Synchronous Motors with Extended State Observer," *Applied Sciences*, vol. 14, no. 18, p. 8359, Sept. 2024, https://doi.org/10.3390/app14188359.
[36] X. Zhang and T. Yuan, "Model Predictive Current Control With Specific Harmonic Suppression for PMSM Drives," *IEEE Transactions on Industrial Electronics*, vol. 72, no. 11, pp. 11070–11080, Nov. 2025, https://doi.org/10.1109/tie.2025.3559954.
[37] S. T. Bahar and H. Qiu, "Amelioration of Traditional PI Boost Converter Utilizing Linear Active Disturbance Rejection Controller - Mode Predictive Control Strategy," *International Journal of Robotics and Control Systems*, vol. 6, no. 1, pp. 305–323, Jan. 2026, https://doi.org/10.31763/ijrcs.v6i1.2364.
[38] W. Zhang, Y. Xu, H. Huang and J. Zou, "Vibration Reduction for Dual-Branch Three-Phase Permanent Magnet Synchronous Motor With Carrier Phase-Shift Technique," in *IEEE Transactions on Power Electronics*, vol. 35, no. 1, pp. 607-618, Jan. 2020, https://doi.org/10.1109/TPEL.2019.2910311.
[39] T. Luan, Z. Wang, Y. Long, Z. Zhang, Q. Li, Z. Zhu, and C. Liu, "Multi-virtual-vector model predictive current control for dual three-phase PMSM," *Energies*, vol. 14, no. 21, p. 7292, 2021, https://doi.org/10.3390/en14217292.
[40] M. Furmanik, M. Vidlak, and P. Rafajdus, "Current Harmonics Control in Six-Phase PMSM," in *2022 ELEKTRO (ELEKTRO)*, pp. 1–5, 2022, https://doi.org/10.1109/elektro53996.2022.9803632.
[41] C. Huang, L. Zhou, Z. Cao, and G. Yao, "Fault-Tolerant Control Strategy with Asymmetric Phase Currents for Single to Four-Phase Open-Circuit Faults of Six-Phase PMSM," *Energies*, vol. 14, no. 11, p. 3163, May 2021, https://doi.org/10.3390/en14113163.
[42] Y. Sun and Z. Wang, "Common-Mode Voltage Suppression for Asymmetrical Six-Phase PMSM Drive System," in *IECON 2023- 49th Annual Conference of the IEEE Industrial Electronics Society*, pp. 1–6, 2023, https://doi.org/10.1109/iecon51785.2023.10312155.
[43] M. Gu, Z. Wang, K. Yu, X. Wang, and M. Cheng, "Interleaved Model Predictive Control for Three-Level Neutral-Point-Clamped Dual Three-Phase PMSM Drives With Low Switching Frequencies," *IEEE Transactions on Power Electronics*, vol. 36, no. 10, pp. 11618–11630, Oct. 2021, https://doi.org/10.1109/tpel.2021.3068562.
[44] S. T. Bahar and R. G. Omar, "Torque ripple alleviation of a five-phase permanent magnet synchronous motor using predictive torque control method," *International Journal of Power Electronics and Drive Systems (IJPEDS)*, vol. 13, no. 4, p. 2207, Dec. 2022, https://doi.org/10.11591/ijpeds.v13.i4.pp2207-2215.
[45] Z. Wang, X. Wang, X. Yang, C. Wen, Y. Gong, and Y. Hu, "Mitigation of DC-Link Current Ripple for Dual Three-Phase Flux-Adjustable Hybrid PMAC Drives Using Collaborative Switching Strategy," in *IEEE Transactions on Industrial Electronics*, vol. 67, no. 9, pp. 7202-7216, Sept. 2020, https://doi.org/10.1109/TIE.2019.2945213.
[46] R. Jiang, Z. Wang, J. Yang, and Z. Chen, "Speed Tracking Control of Permanent Magnet Synchronous Motor via an Active Disturbance Rejection Control (ADRC) Algorithm," *2024 IEEE 6th International Conference on Power, Intelligent Computing and Systems (ICPICS)*, pp. 1632-1636, 2024, https://doi.org/10.1109/ICPICS62053.2024.10796777.
[47] Q. Zhang, H. Pan, Z. Wang, X. Xu, and D. Zeng, "Torque Increase Strategy of Dual Three-phase Permanent Magnet Synchronous Motor Based on VSD Model Harmonic Current Injection," in *2022 25th International Conference on Electrical Machines and Systems (ICEMS)*, pp. 1–6, 2022, https://doi.org/10.1109/icems56177.2022.9982983.
[48] M. Cao, G. Sun, Z. Wu and S. Lu, "Research on Position Sensorless Torque Ripple Suppression Method for Six-Phase PMSM," *2024 International Conference on Intelligent Ships and Electromechanical System (ICISES)*, pp. 191-195, 2024, https://doi.org/10.1109/ICISES64179.2024.11116598.
[49] Z. Wang, K. Yu, Y. Li, and M. Gu, "Position Sensorless Control of Dual Three-Phase IPMSM Drives With High-Frequency Square-Wave Voltage Injection," *IEEE Transactions on Industrial Electronics*, vol. 70, no. 10, pp. 9925–9934, Oct. 2023, https://doi.org/10.1109/tie.2022.3222683.

[50] R. Borase, S. Pawar, and A. Khandekar, "Speed Control of Permanent Magnet Synchronous Motor Using ADRC Technique," *2024 IEEE International Conference on Smart Power Control and Renewable Energy (ICSPCRE)*, pp. 1-4, 2024, https://doi.org/10.1109/ICSPCRE62303.2024.10675219.